Airborne spectroscopic observations of chlorine activation and de-nitrification of the 1999/2000 winter arctic stratosphere during SOLVE

M.T. Coffey, William G. Mankin and James W. Hannigan

National Center for Atmospheric Research

Boulder, Colorado

G. C. Toon

Jet Propulsion Laboratory

Pasadena, California

(Submitted to *J. Geophys. Res.* , July 2001)

Abstract

We have used Fourier transform spectrometers aboard the NASA DC-8 and on balloons as part of the SAGE III Ozone Loss and Validation Experiment (SOLVE) to record infrared absorption spectra of the polar stratosphere. From the high resolution aircraft spectra we derived vertical column amounts of HCl, HF, NO_2, HNO_3 , and a number of other gases for 11 flights in the region of the northern polar vortex. Vertical mixing ratio profiles are derived for a number of gases from two balloon flights. Within the vortex, where low values of total ozone are observed during the latter part of the observation period, we observed markedly reduced columns of HCl and NO_2, and elevated columns of HF and HNO_3 relative to columns outside the vortex. The low value for the ratio of HCl to HF indicates that HCl had been chemically or physically removed, probably providing a source for active chlorine. High values of HNO_3 inside the vortex indicate that nitrogen oxides, which might otherwise mitigate chlorine-catalyzed ozone destruction, have been converted into more stable reservoirs. Because of incorporation into particles some nitric acid may be removed from the stratosphere altogether.

Introduction

The primary objective of SOLVE, driven by observations that ozone losses in the Arctic are becoming comparable to Antarctic losses, is to understand better the processes that control polar stratospheric ozone levels.   Current models do not adequately explain the magnitude of the ozone losses [Chipperfield et al., 1996; Guirlet et al., 2000; Lefèvre et al., 1994].   The focus of SOLVE was on the observed changes in winter ozone at high latitudes, and the concomitant chemical and dynamical processes producing ozone loss, particularly processes that activate chlorine and denitrify the stratosphere. Determination of the physical and chemical nature of polar stratospheric clouds and how they affect chlorine activation was a particular goal. Using the sun as an infrared source, we can measure the high resolution absorption spectrum of the atmosphere and derive the column amount of gases above the aircraft; ozone and about twenty other gases can be measured.   We also can record, at lower resolution but with higher signal-to-noise ratio, broadband infrared absorption of PSCs.   These spectra may allow

identification of the composition and quantification of the amount of PSCs [Glandorf et al., 2002]. For gases with lifetimes long compared to zonal transport times, correlation of column with potential vorticity at several levels allows reconstruction of the field of column amounts throughout the vortex [Coffey et al., 1999].

Instrumentation

The NCAR spectrometer previously has been flown on the DC-8 in the polar campaigns AAOE, AASE, and AASE II; it was extensively refurbished and improved for SOLVE, since the earlier descriptions by Mankin [1978] and Mankin and Coffey [1989]. Only a brief description of the instrument, as modified, will be given here; a fuller description with performance data will be published elsewhere. For our purposes, it suffices to say that the modifications improved the signal-to-noise ratio in the spectra by a factor of 3 to 5 for narrow band ($\sim$500 cm^{-1}) spectra, and even more for broad band ($\sim$2000 cm^{-1}) spectra, and made the background level of the spectra much more stable.

The instrument is a Fourier transform spectrometer, operating at wavelengths of 2-13 μm. It is built around a commercial Michelson

interferometer of the rapid-scanning type. The original plane mirrors have been replaced with precision cube corner reflectors; this improves the stability of the alignment of the modulator in the aircraft vibration environment. The maximum optical path difference of the beams in the interferometer is 16.6 cm, leading to an apodized spectral resolution of 0.06 cm^{-1}.

Solar infrared radiation enters the DC-8 through a 20 cm diameter zinc selenide window, which is transparent from 0.5 to 15 µm. The radiation is directed into the interferometer by a two-axis tracker. Infrared radiation exiting the interferometer is focused on a selectable field stop and passed through one of eight interference filters before being reimaged on the detector. The normal detector is a sandwich of two elements, the front one being photovoltaic indium antimonide (InSb) (for wavelengths less than 5.5 µm) and the rear one being photoconductive mercury cadmium telluride (HCT) (for wavelengths between 5.5 and 14 µm). The second detector failed during the mission, so recording long wave spectra required physically installing an individual HCT detector and dewar and the loss of convenience of the sandwich detector. A spectrum at the maximum resolution requires about 5 seconds to record.

The output of the detector is amplified by a programmable gain amplifier and filtered by a low-pass electrical filter to reduce the noise that could be aliased into the spectral band pass by sampling. It is sampled at the wavelength of a HeNe laser and digitized by a 16 bit A/D converter. After the large signal near zero path difference is recorded, the gain is increased by a factor of 8; this results in an effective resolution of 19 bits in the conversion, producing negligible digitizing noise, typically less than 0.1% in the spectrum.

A laptop computer controls the operation of the interferometer through serial communication with a custom controller board, and collects the digitized samples and saves them on disk. The production of spectra from the interferograms is currently performed on the ground after flight.

The JPL MkIV spectrometer [Toon, 1991] had two balloon flights during SOLVE, on 3 December 1999 and 15 March 2000, when it observed infrared spectra which was used to derive vertical profiles of a number of gases [Toon et al., 2002].

Observations

The Fourier transform spectrometer aboard the DC8 aircraft, described above, made observations during 11 flights of the second and third deployments of the SOLVE campaign. During most of those flights the time available for solar observation was limited to a relatively short period of the flight, as shown in Table 1. During the periods of solar observation the NCAR spectrometer observed the rising or setting sun while viewing in a southward direction from the DC-8 flight path. For the solar elevations encountered the significant absorption along the line-of-sight occurs at some distance south of the aircraft. For a 4 degree solar elevation the line-of-sight intercepts an altitude of 20 km at a distance of 100 km from the aircraft, which is the appropriate point for location of the column observations.

For SOLVE the DC-8 was based in Kiruna, Sweden and flew missions of typically ten hours over the North Atlantic and Arctic oceans, penetrating deep into the polar vortex and often finding PSCs in the coldest regions. We recorded more than 3000 stratospheric solar spectra between 16 January and 13 March, 2000. Figure 1 is an

example of a stratospheric spectrum containing absorption by HCl and CH_4. During the January observations, PSCs were plentiful and most of the observations were made with low resolution (0.5 cm^{-1}) to produce very high signal-to-noise ratio spectra to measure accurately the extinction by PSCs [Glandorf et al., 2002], with some high resolution spectra for determination of column amounts of gaseous species for correction for gaseous extinction. During the March observations there were few PSCs during the solar observations and spectra were mostly made at maximum resolution (0.06 cm^{-1}) to measure column amounts of the gaseous species.

SOLVE 03/09/00 15:08:09

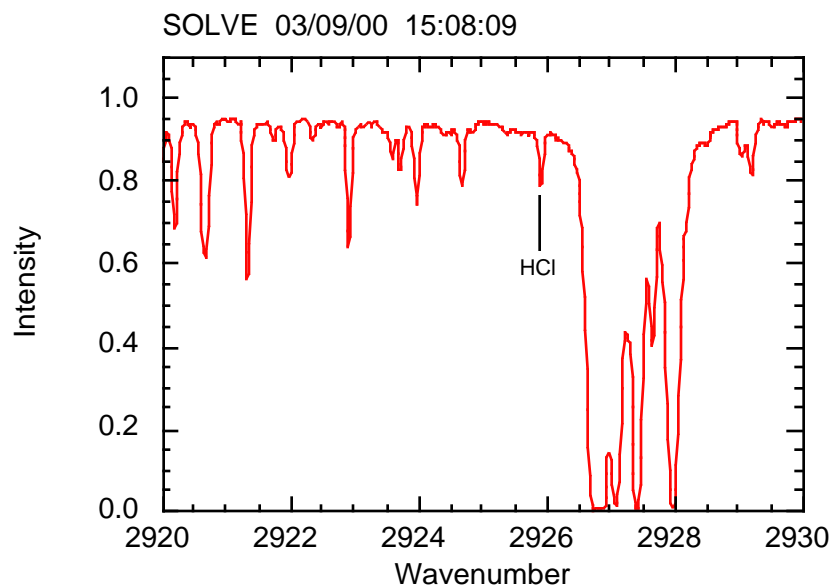Figure 1.   Example of a spectrum from SOLVE representing about 50 sec of observation.

Analysis and results

Processes that activate chlorine and denitrify the stratosphere are of particular interest for their impacts on ozone chemistry. HF is chemically inert in the stratosphere and so serves as a tracer of stratospheric motions. In the winter, wave activity and radiative cooling cause descent of the polar air. Since the HF mixing ratio increases with height, descent, followed by inflow at the upper levels, results in increased columns of HF with increasing latitude and later in the season. HCl, on the other hand, is chemically converted by heterogeneous processes on PSCs. Since its mixing ratio profile is similar in shape to that of HF, if there were no chemical conversion the ratio of HCl to HF would remain constant in the presence of descent, although each would individually increase. Therefore, HCl/HF ratios less than the midlatitude value of around 2.5 show the extent of chemical conversion.

Figure 1 shows a typical aircraft spectrum of HCl that we use for the analysis reported below. We analyzed the spectra by fitting synthetic spectra to the observed spectra and varying the amount of

absorber in the calculation to obtain the best fit. A typical stratospheric profile was used to describe the distribution of gases whose absorption might interfere with the target gas. For January HCl, HF and HNO_3 analysis we begin our fitting with vertical profiles having the shapes of the JPL MkIV observations from December, 1999. To fit the March observations profile shapes are taken from the March, 2000 MkIV observations. The JPL analysis method is described by Toon et al., [1999]. The vertical temperature profile used for January analysis is the average of five January profiles taken from SOLVE meteorological curtain files produced to follow the DC-8 flight track. Similarly, five profiles are averaged for the March temperature profile. Molecular line parameters from the HITRAN database [Rothman et al., 1998] were used to calculate the absorption spectrum. Using the SFIT(Version 1.09) [Rinsland et al., 1982] analysis software the amount of absorber was scaled in a least squares fit to make the calculated lines have the same depth and shape as the observed lines, the scaling factor then is used to compute the line-of-sight amount. Using the shape of the vertical profile and the viewing geometry, line-of-sight amounts are

converted to vertical column amounts above a standard pressure altitude of 200 mb.

Uncertainty in line parameters and atmospheric models are major sources of systematic error in our analysis method. Errors in line intensity scale linearly in retrieved amount, but errors in the line-broadening coefficients and their temperature variation affect the result in a more complex manner, depending upon how strongly the atmosphere absorbs in the line. Uncertainty in the assumed atmospheric temperature can also introduce errors in both intensity and line width. Line parameter uncertainties are estimated to be less than 10% for HNO_3, 5% for HF and 2% for HCl [Rothman et al., 1998, and references therin]. Estimates of column uncertainties due to systematic errors in the vertical profile shapes of HF, HCl and HNO_3 are between 5% and 8%. Total systematic uncertainty in the determination of vertical column amounts are estimated at 9% for HCl, 8% for HF and 12% for HNO_3.

Ertel's potential vorticity (PV) is conserved over moderate time scales, and provides an indication of the location of the vortex. We

use PV on the 440 K isentropic surface to define the vortex morphology. Because of the limited solar viewing time no single solar observation period covered the range of values of PV. Also, during SOLVE, only limited data were obtained outside the vortex, since most of the flight time was spent searching for PSCs in the cold, inner part of the vortex. The solar observing part of the flight of 27 January provided observations which start outside the vortex edge (the vortex edge, near the peak gradient in PV, is usually close to a value of 2.5 $X10^{-5}$ K m^2/kg s) and crossed into the vortex. Figure 2 shows column values of HCl and HF versus PV; the effect of the descent on the columns, especially of HCl near the vortex edge, are plainly evident.
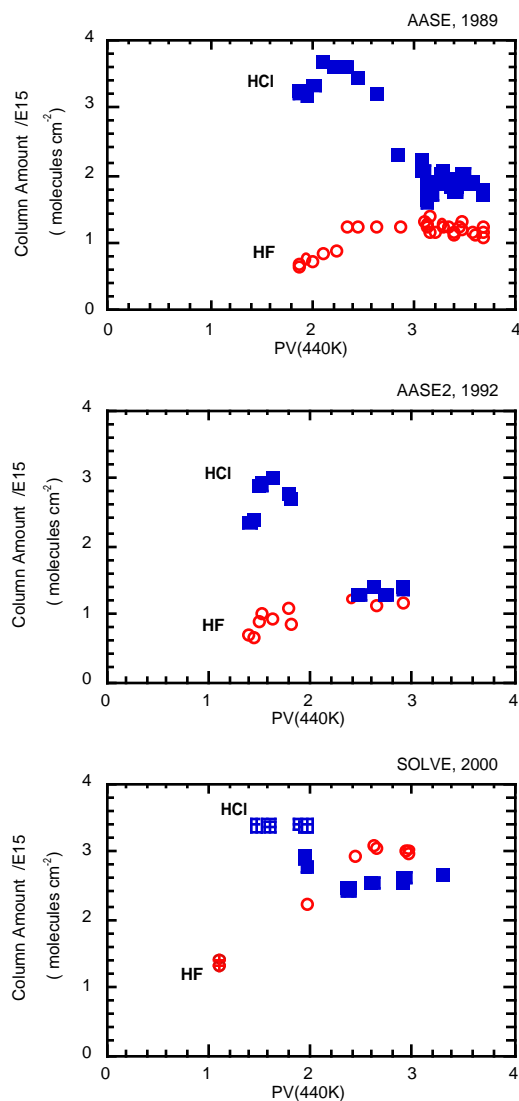
Figure 2. Vertical column amounts of HCl and HF above 200 mb versus potential vorticity on the 440K surface for three winter observation periods AASE(1989), AASE2(1992) and SOLVE(2000). The SOLVE observations are from 27 and 29 January, 2000 which include measurements inside and outside the vortex.
27 Jan: m,n; 29 Jan: ⊕,σ

Figure 3 shows the HCl/HF ratio similarly plotted. Each symbol in Figure 3 represents the average of a number of retrieved columns of HCl and HF for a given day. Observations outside the vortex are averaged together as are values inside the vortex. The ratio of HCl to HF is then calculated from these averages and plotted versus the average PV value. One observes clearly removal of reservoir chlorine in the form of HCl deep in the vortex. In the deepest part of the vortex, the HF column may exceed the HCl column.
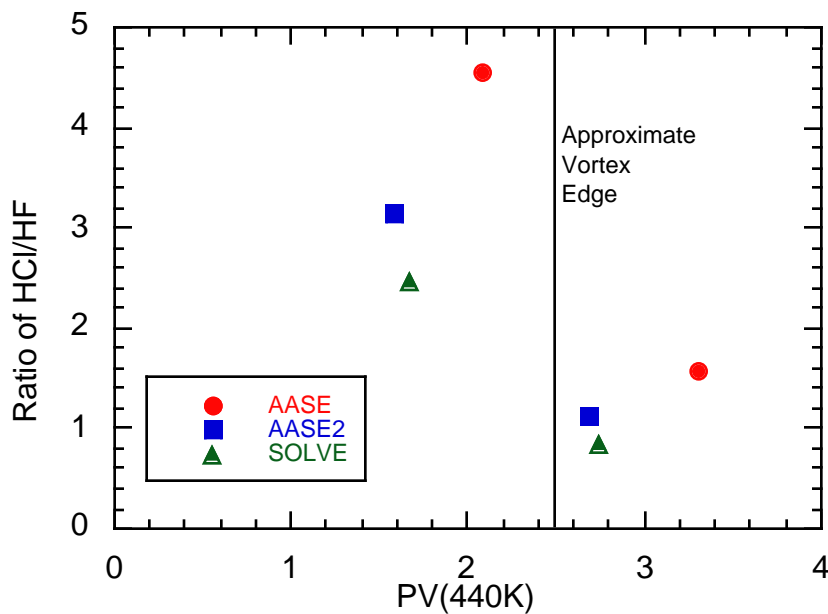

Figure 3. The ratio of HCl column to HF column showing the relative depletion of HCl within the region of the polar vortex for three winter-time observations.

We may assess the extent of HCl destruction within the vortex, and subsequent activation to free chlorine, by comparing the ratio HCl/HF inside and outside the vortex. Comparison of the HCl/HF column ratio for the December balloon observations with the column ratios outside and inside the vortex from the January aircraft observations suggests that some depletion in HCl has occurred outside the vortex boundary and that air within the vortex has been depleted by up to 75% of the HCl column. HCl depletion presumably takes place above about 18 km (the region of lowest temperature, about 190K, begins near 18 km for these days). In the lower stratosphere PSCs may form which provide the sites for reactions which convert HCl to more reactive forms. HCl may react with $ClONO_2$ or with N_2O_5 in PSC particles via:

$$HCl + ClONO_2 \; \ddagger \; Cl_2 \text{ (g)} + HNO_3 \text{ (s)}$$

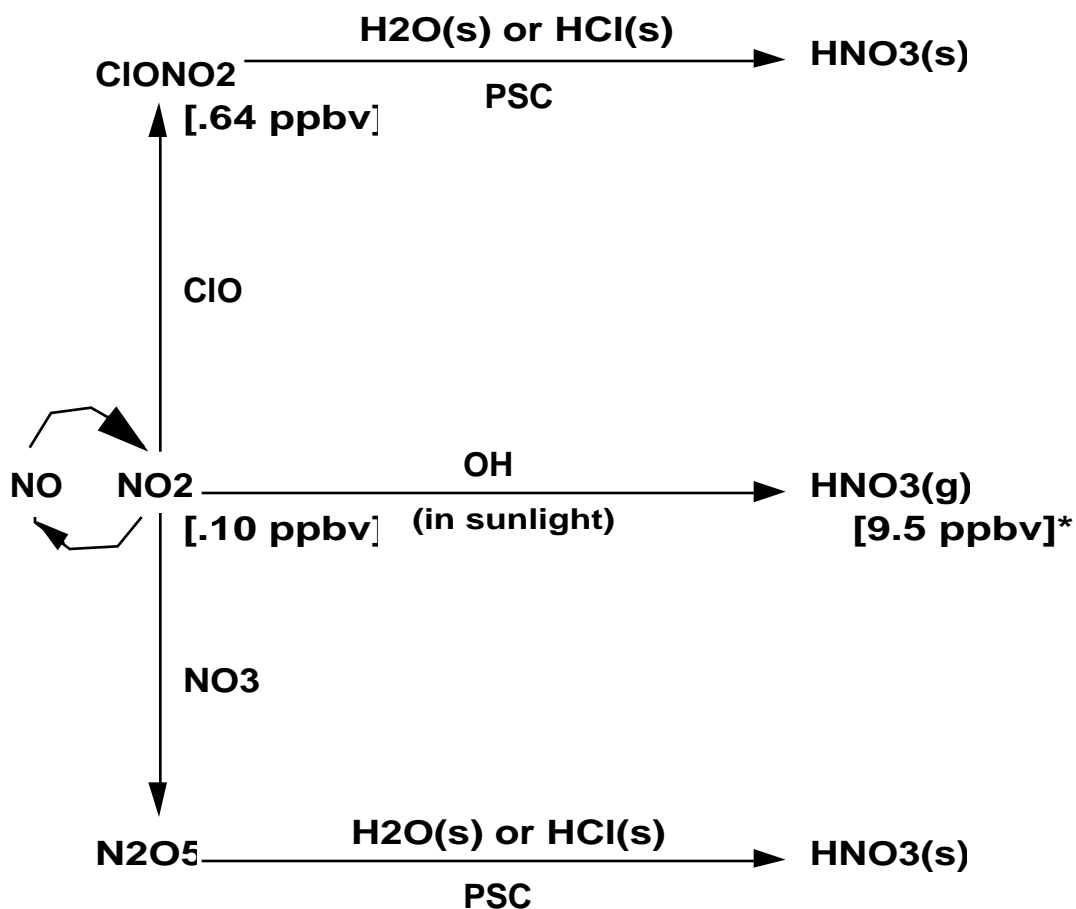$$HCl + N_2O_5 \; \ddagger \; ClNO_2 \text{ (g)} + HNO_3 \text{ (s)}$$

Both these reactions release chlorine in the gas phase which, upon return of sunlight, will photolyze readily to form active ClOx. These

reactions also have the effect of trapping NOy which was in gaseous N_2O_5 or $ClONO_2$ into solid HNO_3 within PSC particles. Nitric acid trihydrate particles have been detected in the arctic winter vortex in two recent studies [Voight et al., 2000; Glandorf et al., 2002]. Taking a pair of days during SOLVE (27 Jan and 29 Jan) we find the HCl/HF ratio within the vortex divided by the ratio outside the vortex to be 0.34. Similar HCl depletion was found during AASE 2 in 1992 (14 and 16 Jan., $(HCl/HF)_{IN}$ / $(HCl/HF)_{OUT}$ = 0.36) and in AASE in 1989 (26 and 29 Jan., 0.35). Thus the activation of chlorine in the 1999/2000 arctic winter was substantial but not very different from two previous winters, even though the 1999/2000 winter was colder than usual and PSCs were more abundant.

A critical component of excess ozone destruction is the availability of reactive chlorine which can act in a catalytic ozone removal cycle. A second critical component necessary for widespread ozone depletion is the removal of nitrogen oxides, NO and NO_2, from the stratosphere. If these compounds are present they will return some ClO to the chlorine reservoir $ClONO_2$. Nitric oxide, NO, and nitrogen dioxide, NO_2, are in a steady state in the lower stratosphere which

depends on ozone concentration and sunlight. In the darkness of polar night this steady state is shifted toward NO_2. NO_2 may react with OH, in sunlight, to form the relatively long-lived reservoir HNO_3. NO_2 also may react with ClO and NO_3 (in darkness) to form the reservoir species $ClONO_2$ and N_2O_5. In the presence of polar stratospheric cloud particles the nitrogen reservoirs, N_2O_5 and $ClONO_2$, can react with H_2O or HCl to deposit odd nitrogen in the particles as solid HNO_3, as described above. Figure 4 shows a diagram of the partitioning of HNO_3 at 20 km in the polar vortex and the major pathways to HNO_3 formation.

ClONO2 **[.64 ppbv]** $\xrightarrow[\text{PSC}]{\text{H2O(s) or HCl(s)}}$ HNO3(s)

ClO ↑

NO ⟷ NO2 **[.10 ppbv]** $\xrightarrow[\text{(in sunlight)}]{\text{OH}}$ HNO3(g) **[9.5 ppbv]***

NO3 ↓

N2O5 $\xrightarrow[\text{PSC}]{\text{H2O(s) or HCl(s)}}$ HNO3(s)

* VMR at 20 km from MkIV Dec 1999 Observations

Figure 4.   Diagram of the partitioning of NOy in the arctic polar vortex near 20 km altitude. The concentration values for gaseous species are from observations by the balloon-borne JPL MkIV spectrometer in December 1999 near 65 N.

Solid HNO$_3$ cannot be detected by the infrared absorption technique used for measurement of gaseous HNO$_3$, described here. If the particles become sufficiently large and fall from the stratosphere the stratosphere is said to be denitrified. Falling particles may be sufficiently warmed at lower altitudes to evaporate and return HNO$_3$ to the gas phase thus effecting a redistribution of gaseous HNO$_3$. If the particles remain in the stratosphere they become a source for NO$_2$, since, when sunlight and warmer temperatures return in the spring, HNO$_3$ is released from the particles to be photolyzed back to NO$_2$.

In the polar winter the predominant nitrogen oxide is HNO$_3$, as illustrated in Figure 5 which shows the vertical mixing ratio profiles of all significant nitrogen oxide species near 65 N in December 1999. HNO$_3$ accounts for more than 90% of NOy (defined as [NO]+[NO$_2$]+2[N$_2$O$_5$]+[ClONO$_2$]+[HNO$_3$]) for altitudes between 10 and 25 km. Thus the fate of lower stratospheric nitrogen oxide is largely that of HNO$_3$.
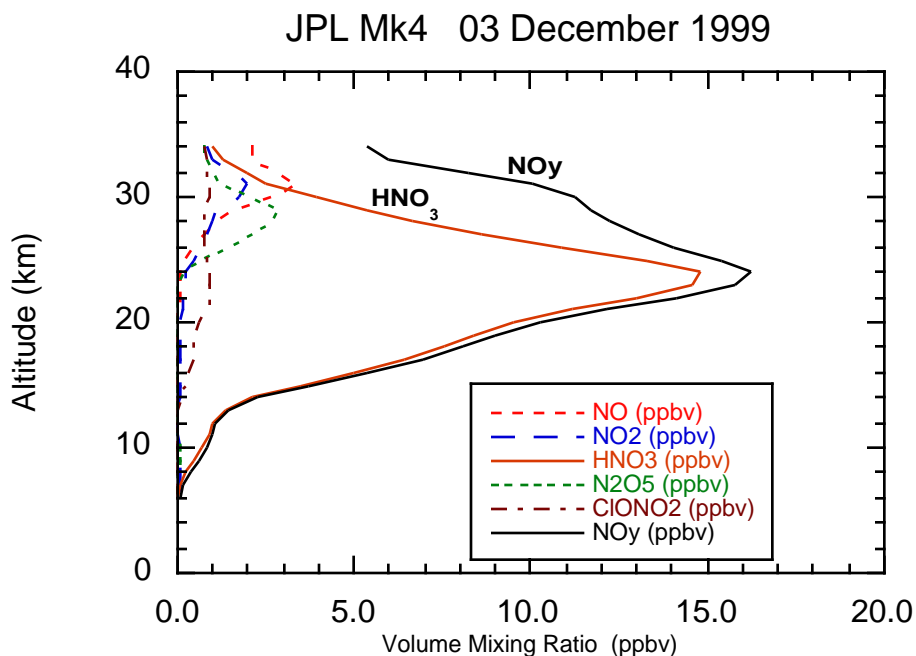
Figure 5.   Vertical mixing ratio profiles of the components of NOy within the polar vortex in December, 1999.

Relatively large amounts of HNO_3 may accumulate in the polar winter stratosphere as illustrated in Figure 6 which shows infrared observations of the gas phase HNO_3 column amount above 200 mb (approximately 12 km) versus potential vorticity on the 440K surface for three winter-time observation periods (AASE, 1989; AASE2, 1992; and SOLVE, 2000).   Nitric acid column amounts increase within the polar vortex due to vertical descent and as NO_2 reacts to form $HNO_3(g)$ and also as $ClONO_2$ and N_2O_5 are converted to $HNO_3(s)$ on PSC particles and subsequently to $HNO_3(g)$.   The solid

HNO$_3$ may be released from the particles, and returned to the

gaseous form, if cloud particles are warmed.

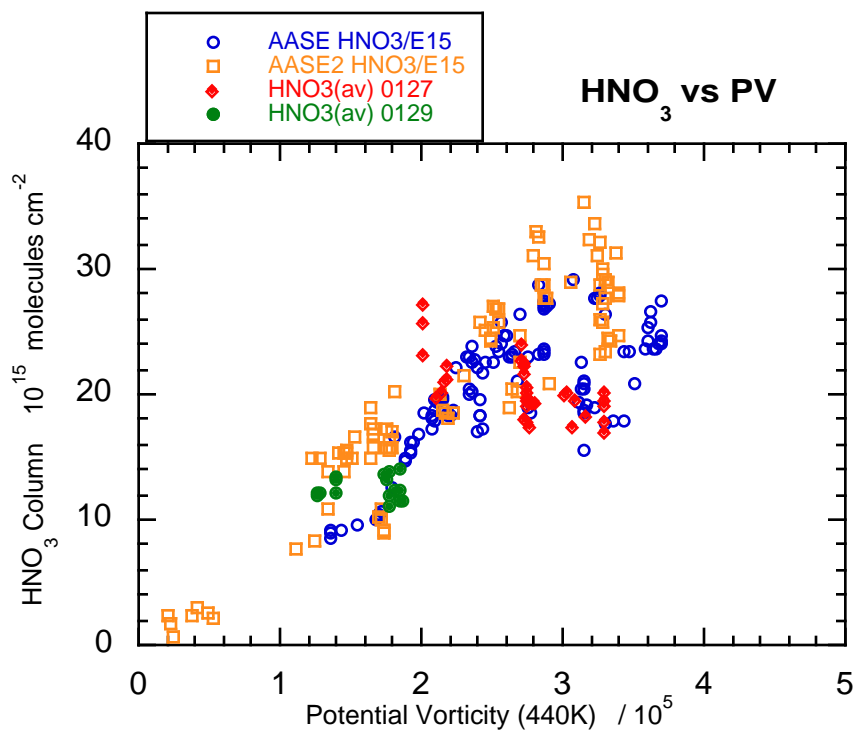

Figure 6.   Column abundance of HNO$_3$ versus potential vorticity on the 440 K surface from January observations made during three field programs AASE(1989), AASE2(1992) and SOLVE(2000).

Balloon-borne in situ measurements in January 2000 (Voight et al., 2000) have shown PSCs in the altitude range from 21 to 24 km to be composed of nitric acid trihydrate (NAT). Those mass spectrometer

measurements indicate that in the lower stratosphere the particles contain approximately the same concentration of HNO_3 molecules as does the gas phase ($\sim 1 \times 10^{10}$ molecules cm^{-3} near 20 km; $\sim$ 5 ppbv). Thus about 50 % of the available NOy (mainly as HNO_3) is contained in the solid (PSC) state. There has been some suggestion that relatively large PSC particles ($\sim$15 μm diameter) may have formed over extensive areas of the 1999-2000 Arctic winter vortex (Fahey et al., 2001). Such large particles would have the effect of transporting HNO_3 from the cold formation altitudes to lower, warmer altitudes as the large particles fall. Such a redistribution of HNO_3 has been modeled in a 4 week simulation (Tabazadeh et al., 2001) which showed a significant removal of HNO_3 above about 18 km and an increase in HNO_3 below, relative to the initial vertical distribution. This vertical redistribution is in substantial agreement with the change in HNO_3 profile observed by the MkIV spectrometer between Dec., 1999 and Mar., 2000, as shown in Figure 7. It should be noted that gaseous, vertical descent in the region from 15 to 30 km between the December and March observations is a major factor in the HNO_3 distribution. It would be a mistake to interpret the

profiles of Figure 7 as simply de-nitrification above 16 km and re-nitrification below.
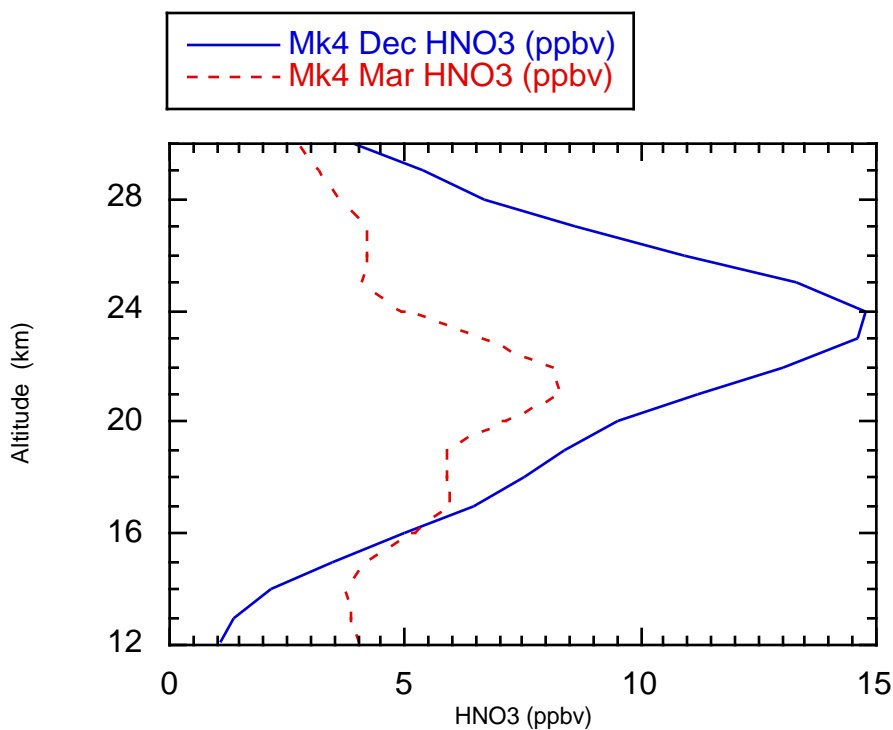

Figure 7.   Nitric acid mixing ratio profiles between 12 and 26 km for December, 1999 and March, 2000 showing the redistribution of HNO_3 inside the polar vortex.

The change in vertical column amount between 12 and 26 km for the two profiles of Figure 7 represent only an 8% decrease from Dec., 1999 to Mar., 2000. Thus, total column measurements are not sensitive indicators of a redistribution of gaseous HNO_3, via

entrapment in falling particles and later evaporation. However, if gaseous HNO_3 is just sequestered in the solid phase, without falling, or if a particle completely falls from the atmosphere then the column amount will be decreased. If 50% of the gaseous HNO_3 between 18 and 26 km were trapped in particles small enough to remain suspended near their creation altitude then the observed column amount would decrease by 30-40 %. Such decreases in HNO_3 column are not observed in our SOLVE observations when compared with previous winter observations, which implies a redistribution of HNO_3 and not complete de-nitrification.

Conclusion

Observations of column amounts of HCl and HF above 12 km during January, 2000 show a substantial reduction in HCl amount (up to 50%). The HCl depletion is similar to that of two previous winter-time observations even though the 1999-2000 winter was colder than usual and PSCs were more abundant.

Column amounts of HNO_3 are increased inside the polar vortex as HNO_3 becomes the major NOy reservoir. There may be significant

redistribution of HNO_3, with removal from altitudes between 18 km and 26 km and enhancement below 18 km as particles fall and vaporize.

Acknowledgments

References

Chipperfield, M. P., A. M. Lee, and J. A. Pyle, Model calculations of ozone depletion in the Arctic polar vortex for 1991/92 to 1994/95, *Geophys. Res. Lett.*, **23**, 559-562, 1996.

Coffey, M. T., W. G. Mankin, and J. W. Hannigan, A reconstructed view of polar stratospheric chemistry, *J. Geophys. Res.*, **104**, 8295-8316, 1999.

Fahey, D. W., R. S. Gao, K. S. Carslaw, J. Kettleborough, P. J. Popp, M. J. Northway, J. C. Holecek, S. C. Ciciora, R. J. McLaughlin, T. L. Thompson, R. H. Winkler, D. G. Baumgardner, B. Gandrud, P. O. Wennberg, S. Dhaniyala, K. McKinney, Th. Peter, R. J. Salawitch, T. P. Bui, J. W. Elkins, C. R. Webster, E. L. Atlas, H. Jost, J. C. Wilson, R. L. Herman, A. Kleinbohl, and M. von Konig, The detection of large HNO_3-containing particles in the winter Arctic stratosphere, *Science*, **291**, 1026-1031, 2001.

Glandorf, D. L., W. G. Mankin, J. W. Hannigan, M. T. Coffey, S. T. Massie, B. Rajaram, E. V. Browell, O. B. Toon, and M. A. Tolbert, Identification of nitric acid trihydrate (NAT) in the arctic stratosphere using infrared extinction measurements, *J. Geophys. Res.,* **xx**, xxx-xxx, 2002.

Guirlet, M., M. P. Chipperfield, J. A. Pyle, F. Goutail, J. P. Pommereau, and E. Kyro, Modeled Arctic ozone depletion in winter 1997/1998 and comparison with previous winters, *J. Geophys. Res.*, **105**, 22185-22200, September 16, 2000.

Lefèvre, F., G. P. Brasseur, I. Folkins, A. K. Smith, and P. Simon, Chemistry of the 1991-1992 stratospheric winter: Three-dimensional model simulations, *J. Geophys. Res.*, **99**, 8183-8195, 1994.

Mankin, W. G., Airborne Fourier transform spectroscopy of the upper atmosphere, *Opt. Eng.*, **17**, 39-43, 1978.

Mankin, W. G., and M. T. Coffey, Airborne measurements of stratospheric constituents over Antarctica in the austral spring 1987, 1, Method and ozone observations, *J. Geophys. Res.,* **94**, 11,413-11,421, 1989.

Rinsland, C. P., M. A. H. Smith, P. L. Rinsland, A. Goldman, J. W. Brault, and G. M. Stokes, Ground-based infrared spectroscopic measurements of atmospheric hydrogen cyanide, *J. Geophys. Res.,* **87**, 11,119-11,125, 1982.

Rothman, L. S., C. P. Rinsland, A. Goldman, S. T. Massie, D. P. Edwards, J-M. Flaud, A. Perrin, C. Camy-Peyret, V. Dana, J-Y. Mandin, J. Schroeder, A. McCann, R. R. Gamache, R. B. Wattson, K. Yoshino, K. V. Chance, K. W. Jucks, L. R. Brown, V. Nemtchinov, and P. Varanasi, The HITRAN molecular spectroscopic database and HAWKS (HITRAN atmospheric workstation): 1996 edition, *J. Quant. Spectrosc. and Radiat. Transfer*, **60**, 665-710, 1998.

Tabazadeh, A., E. J. Jensen, O. B. Toon, K. Drdla, and M. R. Schoeberl, Role of the stratospheric polar freezing belt in denitrification, *Science*, **291**, 2591-2594, 2001.

Toon, G.C., The JPL MkIV Interferometer, *Optics and Photonics News*, **2**, 19-21, 1991.

Toon, G. C., J.-F. Blavier, B. Sen, J. J. Margitan, C. R. Webster, R. D. May, D. W. Fahey, R. Gao, L. Del Negro, M. Proffitt, J. Elkins, P. A. Romashkin, D. F. Hurst, S. Oltmans, E. Atlas, S. Schauffler, F. Flocke, T. P. Bui, R. M. Stimpfle, G. P. Bonne, P. B. Voss, and R. C. Cohen, Comparison of MkIV balloon and ER-2 aircraft profiles of atmospheric trace gases, *J. Geophys. Res.,* **104**, 26,779-26,790, 1999.

Toon, G. C., J.-F. Blavier, and B. Sen, Remote balloon measurements of chlorine de-activiation, de-nitrification, and ozone loss during the 1999-2000 Arctic winter, *J. Geophys. Res.,* **xx**, xxx-xxx, 2002. [this issue].

Voight, C., J. Schreiner, A. Kohlmann, P. Zink, K. Mauersberger, N. Larsen, T. Deshler, C. Kroger, J. Rosen, A. Adriani, F. Cairo, G. Di

Donfrancesco, M. Viterbini, J. Ovarlez, H. Ovarlez, C. David and A. Dornbrack, Nitric acid trihydrate (NAT) in polar stratospheric clouds, *Science*, **290**, 1756-1758, 2000.

Table 1

Date 2000	DC-8 T/O and Landing Time (UT)	Solar Observation Period (UT)	Obs. Latitude Range N	Obs. Longitude Range	Range of Solar elevation (degrees)
0116	06:49 16:51	10:25 10:37	66.00 67.50	54.00 E 55.00 E	7.00 5.00
0120	08:20 18:06	10:10 10:40	65.08 68.12	10.20 E 19.10 E	6.50 4.20
0123	07:34 17:53	12:20 14:15	68.22 68.31	20.10 E 14.00 W	10.20 0.60
0125	07:31 17:52	13:15 14:45	64.50 66.60	22.03 E 4.00 E	12.10 0.50
0127	09:21 19:03	12:40 15:15	57.47 64.95	32.18 E 2.73 E	7.30 -1.20
0129	08:45 19:32	15:26 17:00	60.95 50.70	106.72 W 113.92 W	12.00 -1.90
0303	14:19 24:18	16:50 18:00	64.10 73.22	2.03 W 8.15 W	10.30 1.10
0305	10:48 20:21	12:20 13:15	75.10 78.02	37.20 E 11.04 E	6.04 0.02
0308	08:16 18:56	11:45 13:17	68.18 77.20	71.63 E 57.58 W	4.60 -0.60
0309	13:48 23:43	14:37 16:06	71.67 80.05	16.00 E 13.47 W	6.90 2.90
0313	14:47 23:39	17:10 18:10	69.98 77.07	3.23 W 0.28 W	4.10 -2.20